6th annual IEEE Conference on Automation Science and Engineering
Marriott Eaton Centre Hotel
Toronto, Ontario, Canada, August 21-24, 2010

Automated Surface Deformations Detection and Marking on Automotive Body Panels

Valentin Borsu, Arjun Yogeswaran, and Pierre Payeur

Abstract— **This paper proposes an integrated solution for automated surface deformations detection and marking on automotive body panels in the context of quality control in industrial manufacturing. Starting from a 3D image of the surface of the panel, deformations are extracted and classified automatically. The positions of the surface defects are provided to a robotic marking station that handles pose and motion estimation of the part on an assembly line using passive vision. The integrated system is validated with an experimental setup, using an automobile car door panel.**

I. Introduction

Quality control in the manufacturing industry has traditionally been performed manually by workers. However, with advances in computers, robotics, and sensor technologies, automated inspection is quickly penetrating this area of operation, resulting in more accurate, efficient, safe and cost effective solutions. In the automotive industry, quality control is critical to ensure that automotive body parts meet predefined standards. Identifying deformations, such as undesired dings and dents on panels, and marking them so that they are repaired while still on the assembly line is essential. In current industrial settings, the procedure for identifying surface defects on automotive body panels often requires a laborious manual surface rubbing operation. Identified deformations are also manually marked with washable ink over the part.

To achieve fully automated panel inspection, feature extraction is preferably performed over 3-dimensional data. However, most approaches are best suited for determining features at a single resolution, and target defects of a specific size or scale [1]. Due to the possibility of deformations being of variable sizes, and because of variations in the sampling density of the scanner, feature extraction techniques usually rely on adaptive thresholds and variable levels of sensitivity to operate in different manufacturing scenarios. To accommodate a wider range of operational requirements, effective feature extraction methods have been proposed that use multiple independent passes to generate multi-resolution representations [2, 3]. While the techniques can provide accurate results, they also remain computationally expensive. The method developed in this work for feature extraction and classification directly handles features at various scales. It builds on an octree data structure to efficiently represent the multi-resolution features, and permits the grouping of local features to aid in the classification.

On the other hand, autonomous marking of the locations where deformations appear over an automotive body panel, with a robotic system, requires that the pose and motion of the panel on the assembly line is accurately estimated. Under the general constraints of car manufacturing, the panel is either translating or rotating, describing a smooth and continuous motion. In most cases, the automotive body panels are unfinished at the stage of inspection. Therefore the texture and color properties of the surface are not strongly contrasting or easily detectable to help in solving the pose estimation problem. Additionally, the pose estimator needs to run without any exact CAD model of the panel, in order to maximize flexibility.

Yoon *et al.* [4], and Chang *et al.* [5] pointed out the difficulties met in the cases of tracking and interacting with industrial bodies, which often suffer from a lack of prominent features. For pose estimation, the literature provides a number of alternatives to the feature extraction and matching problems [6, 7, 8, 9]. However, the reliability of these techniques on unfinished automotive body panels is highly affected by the lack of sharp and unique features visible over the surface. Therefore, given the operational constraints mentioned above, and the need to operate in real-time, a feature-based tracking technique is privileged for pose estimation of the panel. The technique relies on a pre-selected set of geometrical features associated with the panel's structure that can be uniquely identified and consistently tracked on an image-by-image basis, along the inspection workcell. The feature tracking technique was introduced in [10] and uses the pyramidal implementation [11] of the Lucas-Kanade (LK) tracker [12]. The proposed approach combines a feature tracker with a calibrated stereo-vision system. This eliminates the restrictions imposed on the types of motion that the panel might exhibit on the assembly line. As a result, a higher level of generality is achieved, when compared to other techniques [13, 14] that impose constraints on the movement of the tracked object.

This paper builds upon initial versions of the pose and motion estimation algorithm [10] and the deformation detection method [15]. It details the integration of the various components that allow for scanning an automotive body panel, detecting undesired deformations over its surface, and marking the defects using a robotic arm, without human intervention beyond initialization. It also presents the validation of the automated inspection station.

The authors acknowledge the financial support from Precarn Inc., and the collaboration of Neptec Design Group Ltd and Honda Canada to this research.

V. Borsu, A. Yogeswaran, and P. Payeur are with the School of Information Technology and Engineering, University of Ottawa, ON, Canada, K1N 6N5; e-mail: {vbors100,ayoge099,ppayeur@site.uOttawa.ca}

Section II introduces the framework for the automated deformations detection and marking system. Sections III and IV detail the deformation detection and marking algorithms. In Section V, the experimental validation of the system is detailed and analyzed.

II. Integrated Solution and Experimental Platform

The major components of the proposed deformations detection and marking framework are shown in Fig. 1. A structured light sensor (SLS) [16] generates a colored dense 3D reconstruction of the surface profile of the panel. It uses a stereoscopic pair of cameras and projected lighting under the form of a bi-dimensional pseudo-random color pattern which is scrolled over the surface. The pattern projected onto the unfinished metallic panel creates a set of artificial feature points that compensate for the lack of prominent ones. The 3D data acquisition setup is illustrated in Fig. 2.

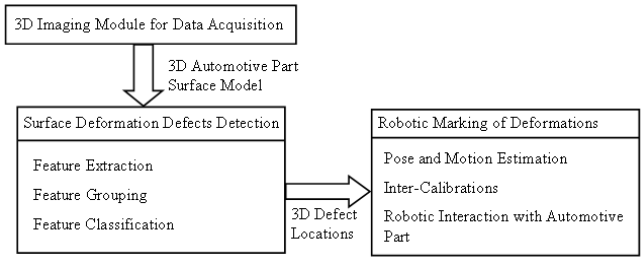

Fig. 1. Proposed deformations detection and marking framework.

The 3D surface model of the automotive part represents the input to the surface deformations detection subsystem which focuses on 3D feature extraction, grouping and classification. The output of this subsystem maps the 3D locations of the surface deformations, expressed with respect to the left camera, $CamL_{SL}$, of the SLS.

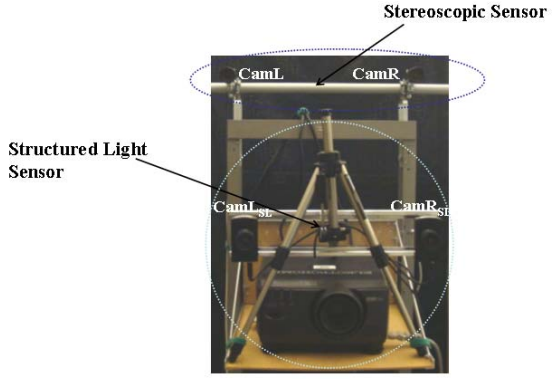

Fig. 2. Surface modeler (SLS) and pose estimator (stereoscopic) used for robotic guidance.

The robotic marking subsystem estimates the pose and motion of the panel on the assembly line, and performs the path planning to guide the marking. In order to guarantee consistent movements between the inspected panel and the robot's end-effector, two inter-calibrations are performed. The first one involves the computation of the rigid transformation between the left camera (CamL) of the stereoscopic sensor that monitors the pose of the panel and the base reference frame of the robot, O_B, as shown in Fig. 3b. The second calibration relates CamL with the reference frame of the SLS, $CamL_{SL}$. Since the positions of the surface deformations are obtained with respect to $CamL_{SL}$, the inter-calibrations make it possible to transfer these deformation locations into the robot's reference frame, to guide the marking operation.

In order to reproduce an automotive body panel inspection station in the laboratory, an experimental setup, shown in Fig. 3a, is used that includes a full-scale mock-up car door which is mounted on a 54cm sled system that operates as a short assembly line. The door model reproduces the generic characteristics of any typical car door at an early stage of manufacturing, including a smoothly curved surface as well as the inner and outer frames of the window opening. In addition to this, the door model also features a door handle and some appended deformation defects.

A second stereo-vision system, shown in the upper part of Fig. 2, is located about perpendicularly to the panel surface and provides estimations on the pose and motion of the object in the workcell. The actual interaction with the panel is performed by a 7-DOF F3 CRS manipulator robot, mounted on a 2m track, which is equipped with a pointing tool as shown in Fig. 3b. Figure 3c shows a segment of a frame containing the projection of the pseudo-random pattern onto the scene by the SLS during the data acquisition process. Figure 3d illustrates the resulting textured surface map of the scanned car door.

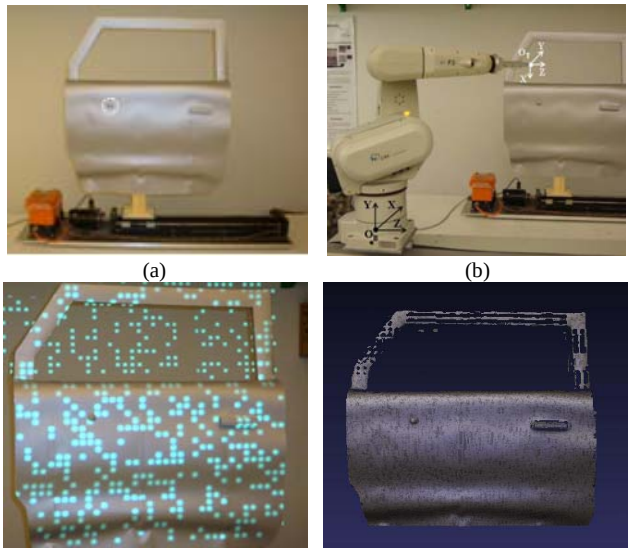

Fig.3. (a) Sled system with car door, (b) F3 manipulator robot with pointing tool, (c) bi-dimensional pseudo-random pattern projected onto car door, (d) textured point set surface map of scanned car door.

III. 3-Dimensional Deformations Detection

The surface deformations detection module takes a 3-dimensional mesh computed from the 3D point cloud generated by the SLS, extracts areas containing 3D features, and classifies them to identify dings and dents over the surface of the object. The detection of deformations operates

in three steps. The first stage extracts local features from the 3D model. The second one groups local features into feature clusters to aid in the third and final stage of classification.

A. Feature Extraction

The feature extraction uses an octree data structure to generate a multi-resolution representation of the 3D mesh [15]. Then, using the standard deviation between surface normals as a metric, it removes uniform surfaces and leaves only the areas containing sharper variations of their normal orientation, indicating potential deformation features.

Variations in the surface of a given region are estimated from the standard deviation of the surface normal vectors within that region. The performance of this algorithm is improved by using the area of each triangle as a weight to calculate the mean normal and standard deviation. This minimizes the effect of small noisy areas, overcomes the effect of non-uniformly distributed 3D points, and provides a more accurate representation of the variations over the region being analyzed. The evaluation of the standard deviation value facilitates the partitioning process, where high values indicate a potential feature, and low values indicate a relatively smooth or ultimately flat surface.

First, the area of each triangle is calculated:

$$a_i = \frac{1}{2}\left|\vec{v}_{i1} \times \vec{v}_{i2}\right| \tag{1}$$

where $\vec{v}_{i1}$ and $\vec{v}_{i2}$ are any two of the edge vectors that define the triangle, T_i, of the mesh. Then, the weighted average normal, $\bar{\vec{N}}$, is calculated, with the areas of each triangle as weights:

$$\bar{\vec{N}} = \sum_{i=0}^{n} \frac{a_i}{A} \vec{N}_i \tag{2}$$

where $A = \sum_{i=0}^{n} a_i$, n is the number of triangles within a node of the octree, and $\vec{N}_i$ is the unit normal of each of the triangles. Finally, the weighted standard deviation, σ, of the normals is estimated as:

$$\sigma = \sqrt{\frac{\sum_{i=0}^{n} a_i (\vec{N}_i - \bar{\vec{N}})^2}{A}} = \sqrt{\frac{\sum_{i=0}^{n} a_i \left[(x_i - \bar{x})^2 + (y_i - \bar{y})^2 + (z_i - \bar{z})^2\right]}{A}}. \tag{3}$$

If, in a given volumetric node of the octree, the calculated standard deviation value is greater than a set threshold, the node is subdivided for further investigation at a higher resolution. The subdivision is realized by adding children to the node being investigated, and redistributing the surface mesh triangles into the children with each child representing a subdivision of the volume. This process is repeated until the tree has reached a maximum depth, corresponding to the finest resolution for the features.

The final structure provides a tree where the surface triangles are distributed amongst the nodes. By retrieving all the nodes at a certain depth, the features at the corresponding scale can be identified by the portions of the mesh contained in the selected nodes.

B. Feature Grouping

After the features are extracted, the tree is analyzed to retrieve local information about the features over the mesh. This local information contains pieces of the deformation features. The feature grouping phase aims at grouping a collection of local feature pieces, at a given scale, to represent an actual larger deformation, such that information about size, shape, and other characteristics of that deformation can be determined, to aid in classification.

The grouping begins by considering only the extracted features at the deepest level of the tree. Given that features are mapped by triangles contained in the nodes, triangles at nodes that do not belong to the deepest level of the tree are removed, and are deemed non-feature triangles.

Proximity determines whether nodes remaining as feature triangles should be connected as part of a feature group. Since each node represents a certain volume occupied by the mesh, any of them may contain some of the triangles that define the surface mesh of the object. Therefore, a relative occupancy, ρ, is defined as the total surface of those n triangles with respect to the overall volume of the node, v, that contains them. The relative occupancy can be calculated as follows:

$$\rho = \sum_{i=0}^{n} \frac{a_i}{v}. \tag{4}$$

At the desired scale, all nodes below a certain threshold of relative occupancy are also removed, such that outliers in the feature extraction are discarded. Remaining nodes that are spatially adjacent are connected, as described in Fig. 4. This algorithm results in several lists, each containing one or more nodes. Each list represents a different deformation feature at the desired scale which can then be classified.

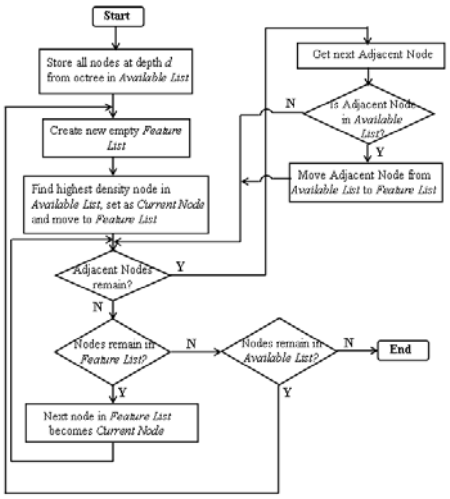

Fig. 4. Grouping of feature nodes in the octree structure.

C. Feature Classification

A feature classifier is designed to identify feature groups that exhibit the characteristics of the deformation features to be detected, such as extra spots of welding, holes, or dings and dents. Deformations are characterized mainly by their

size and surface curvature. The classification phase provides the exact 3D locations of each deformation that is used by the robotic marking system.

IV. Robotic Marking of Deformations

The marking stage integrates the estimation of pose and motion of the door panel with a stereoscopic sensor (Fig. 2), which is precisely calibrated with the robot manipulator and the SLS.

A. Algorithm for Pose and Motion Estimation

Considering the structure of a car door, a set of 10 prominent features, called the macro-features (MFs), are selected. They belong to the inner and outer frames of the door window. These macro-features are subsequently extracted and tracked over a sequence of images. Figure 5 presents a block diagram of the pose and motion estimation algorithm.

The process starts with a rough selection of macro-features by the operator. This step is executed only once at initialization over the first image grabbed by CamR. This initial knowledge gives the system the capability to reconfigure itself when a subsequent door appears on the assembly line. The rough MFs are refined in the first step of the process, *A*, using the two images grabbed by CamL and CamR. The refinement procedure is performed with the Shi and Tomasi corner detector [7] with sub-pixel accuracy, in the image acquired by CamR. Additionally, the refined positions of the macro-features, which form the topological structure of the car door, in the image plane, are saved in a reference buffer.

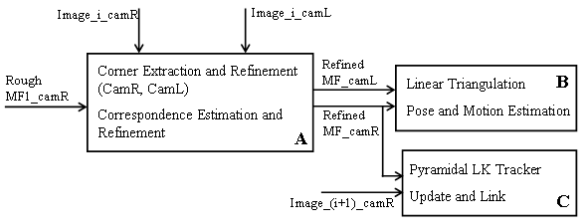

Fig. 5. Proposed pose and motion estimation algorithm.

The pyramidal Lucas-Kanade tracker [11, 12] is used for guiding the correspondences of the macro-features between the two views of the scene. The resulting estimates of the position of the MFs in the CamL image are corrected by applying the corner detector [7] in the image grabbed by the left camera. Following this first estimation, the system can re-initialize the estimates provided by the tracker based on the motion vectors that will be calculated in step *C*.

Once the correspondence problem is solved, a linear triangulation procedure [17] is employed for estimating the 3D position of the macro-features in step *B*. This 3D data provides the input to the pose and motion estimation procedure which computes the rigid transformation that the panel has undergone between two successive images, collected by the stereoscopic camera pair, using least-squares [18]. The following image capture represents the starting point for the computation of the motion vectors for the macro-features, using the pyramidal LK tracker [11, 12], in step *C*. The embedded monitoring stage of the MFs' motion vectors returned by the pyramidal LK tracker [11, 12] relies on the data stored in the reference buffer, which imposes geometric constraints on the distribution of the MFs. It is assumed that the scaling effects of the tracked car door, in the image plane, are minor during the entire motion sequence. As a result, the proposed feature tracking module overcomes the occlusions caused by the robot, and the sensitivity of the LK tracker [11, 12] to illumination changes, shading effects, or the temporary appearance of other objects in the scene. This tracking approach makes the solution suitable for real-time operation. Pose and motion estimation is terminated when the door panel exits the field of view of the cameras.

While an image capture rate of f_{extr}=0.5Hz is sufficient to achieve accurate marking over an assembly line that moves at 1.4cm/s, the pose and motion estimator can operate in real-time up to an update rate of f_u=5Hz, when using two Point Grey Flea2 IEEE-1394a CCD cameras with CCTV 8.5 mm lenses at a resolution of 640x480 pixels.

B. Inter-Calibration of Vision Sensors and Robot

In order for the robot to accurately mark the deformations on the automotive body panel, an inter-calibration must be performed between CamL of the stereoscopic sensor and the robot's base. For this matter, a checkerboard pattern, which can be attached to the gripper, was designed. The calibration pattern is mounted in colinearity with the reference frame of the tool, O_T, as shown in Fig. 6a. Given that the only transformation between the tool of the robot and the calibration pattern is a constant translation along the Z axis of the tool's reference frame (Fig. 2b), the location of the checkerboard corners can be uniquely defined with respect to O_T, and eventually, to the robot base, O_B, knowing the robot's kinematics.

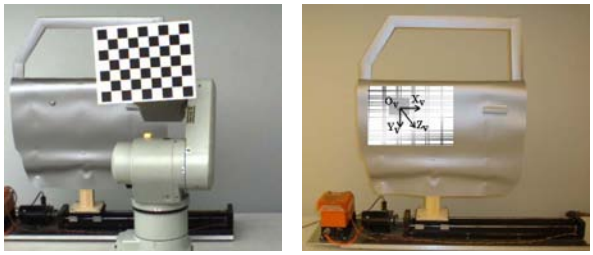

(a) (b)

Fig. 6. (a) Image taken by CamL during the inter-calibration procedure, (b) plane interpolation and reference frame over the deformation area.

To acquire a set of calibration feature points, the robot is successively driven to 15 different configurations such that the region of the workspace containing the automotive body panel over the visible section of the assembly line is covered. For each different robotic configuration, a synchronized set of images is acquired by both cameras, CamL and CamR. The stereo correspondence problem is

solved and the 3D positions of the calibration feature points are recovered, with respect to CamL. The rigid transformation from the robot's base to CamL, Q_{CB}, is computed [18] using the amalgamated 15 datasets.

To achieve the inter-calibration between the SLS used for 3D imaging of the panel surface and the stereoscopic sensor used for pose and motion estimation of the panel, the same methodology, with synchronized data acquisition, is applied.

C. Robotic Pointing of Surface Deformations

The robotic interaction relies on the results provided by the deformations detector and the panel's pose estimator. The robot is used to point the regions with deformations over the door panel. The fact that the locations of the surface deformations are readily provided in the base reference frame of the robot, O_B, after inter-calibrations, simplifies the path planning for the robot to mark the deformations. This generic solution is adequate independently of the marking strategy, including the use of a marker tip or chalk, a stamping sponge or a spray gun.

Beyond the locations of the detected deformations, the orientation of the marking tool, with respect to the area that the robot needs to point to, must also be specified. For that matter, a least-squares interpolation of a plane is computed from a set of 3D points, expressed with respect to CamL, that include the location of the surface defect, and a sub-set of points extracted from the 3D model of the object, acquired with the SLS, by applying uniform 2D sampling over a 3cm x 3cm patch centered over the detected deformation, as shown in Fig. 6b. A supplementary reference frame, O_v, is attached to the computed plane. Its origin is defined by the center of the deformation area, with the X and Y axes parallel to the interpolated plane vectors and the Z axis pointing out of the plane, perpendicularly to the local surface patch. The 3D vectors representing the axes of O_v are normalized to form a rotation matrix that defines the rigid transformation from CamL to the robot's tool, Q_{TC}. The rotation matrix is estimated as:

$$R_{TC} = [\overrightarrow{Y_v} \mid -\overrightarrow{X_v} \mid -\overrightarrow{Z_v}] \quad (5)$$

where the three linear independent columns are selected such that the tool reference frame, O_T, becomes collinear with O_v, except for the Z axes that point in opposite directions. The translation component of Q_{TC} is estimated by the position of the deformation with respect to CamL. Finally, the transformation defining the pointing pose of the tool with respect to the base of the robot, Q_{TB}, is defined by:

$$Q_{TB} = Q_{CB} \cdot Q_{TC.} \quad (6)$$

V. Experimental Validation

The deformations detection module was tested on scans containing 32040 points of the door panel collected with the SLS sensor. A deformation protruding from the model by 1.1cm with a diameter of 0.9cm was added, as well as a door handle extending from the door panel by 1.8cm over a width and height of 10cm and 1.8cm, respectively. Figure 7a presents the results of the feature extraction at a tree depth of 7. The results show that the deformation and the door handle are both extracted from the surface mesh. Various features such as the door curvature near the bottom, and the door frame and contours are also detected at that resolution. Although the deformation and the door handle are of different sizes and depths, the algorithm is able to separate those features from the curvatures and noise in the 3D model. The SLS scanner is capable of many resolutions, and at each resolution, the ability of the system to detect deformations is different. The current configuration of the system allows the detection of deformations at a minimum size of approximately 1cm x 1cm x 1cm. Using a 3D scanner with higher resolution allows detecting finer deformations, without any change to the detection and grouping algorithms.

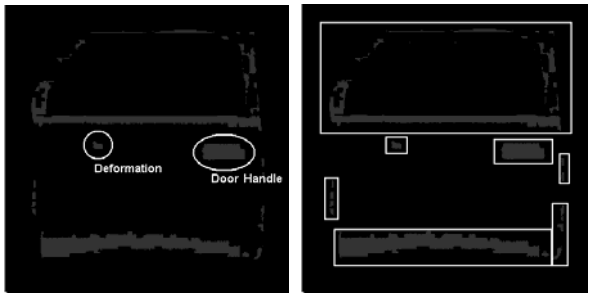

(a) (b)

Fig.7. (a) Feature extraction, and (b) feature grouping results at depth 7.

The feature grouping algorithm is applied at the same tree depth. The results are shown in Fig. 7b, with each of the feature groups being framed. The door handle is grouped as a single feature, and the deformation is also isolated as a separate feature. While other features in the mesh also get grouped, they are removed during the classification stage as they do not meet the size or shape criteria of a deformation of interest, being either too large or too sparse.

To evaluate the performance of the marking system, nine scenarios were considered, based on the pose of the door panel on the assembly line. For experimentation, a constant speed of $v_{sled} \approx 1.4$cm/s was set for the sled system. Performance with three different orientations of the sled was analyzed. These orientations were obtained by rotating the sled system around the Y_v axis (Fig. 6b), with different angles $(\theta_0, \theta_1, \theta_2) = (0^\circ, 10^\circ, -15^\circ)$. For each case, the deformations detection system provided the location of the deformations (w.r.t. $CamL_{SL}$) when the panel was located at the beginning of the assembly line (Pos_A). The pointing operation was performed when the panel was located at the beginning (Pos_A), the middle (Pos_B) and the end (Pos_C) of the sled, each location being separated by 27cm.

To ensure the integrity of the panel during testing, a safety reserve of δ_r=3cm was preserved between the pointing tip and the panel surface. Figures 8a and 8b illustrate the pointing operation in scenarios (PosB, θ_1) and (PosC, θ_2).

In order to monitor the accuracy of the pointing operation, the absolute errors, $|e_x|$, $|e_y|$ and $|e_z|$, characterizing the displacement error of the pointing tip to the center of the deformation, were measured, with respect to the axes of the robot's base reference frame, O_B. Table I presents the errors for the 9 scenarios considered.

(a) (b)

Fig. 8. Deformation pointing results: (a) (PosB, θ_1), (b) (PosC, θ_2).

TABLE I
ACCURACY OF DEFECTS POINTING OPERATION

Absolute Error	POS_A			POS_B			POS_C		
	θ_0	θ_1	θ_2	θ_0	θ_1	θ_2	θ_0	θ_1	θ_2
$\|e_x\|$(cm)	1	0.9	1.1	1.3	1.3	1.4	1.5	1.4	1.6
$\|e_y\|$(cm)	0.7	0.9	1	1.2	1	1.1	1.1	1.2	1.4
$\|e_z\|$(cm)	1.2	1.1	1.2	1.5	1.4	1.5	1.4	1.5	1.5

The errors are fairly uniform in all directions and remain stable independently from the position or orientation of the panel along the track. The principal sources of error come from the limited resolution of the SLS sensor that slightly biases the exact location of the deformation over the panel, and from the accuracy of the pose and motion estimator, together with the rigid transformations estimated via the inter-calibration procedures. The latter two are largely influenced by the fact that the stereoscopic camera system must remain at a relatively large distance (about 3m) from the assembly line in order to provide a sufficiently wide field of view to track the panel over the entire inspection workstation.

The precision achieved in this validation phase makes the approach suitable for marking with a stamping sponge or a spray gun, given that the objective is to mark the region that contains the deformation within a few centimeters accuracy. The exact location of the deformation within the marked region is easily determined by workers who will perform the repair in a separate station, using the marks as guides. For that matter the proposed solution represents a viable alternative to perform fully automated detection and region marking of deformations over large surfaces and for substantial volumes of production.

VI. CONCLUSIONS AND FUTURE WORK

This paper addressed the problem of automated identification and marking of surface deformation defects for quality control in the automotive industry. Starting from a 3-D surface mesh of an automotive part, feature extraction and classification techniques precisely determine the locations of undesired deformations and pass that information to an autoguided robotic marking system. The latter embeds a pose and motion estimator to track an automotive body panel on the assembly line. The experimental validation demonstrated that sufficient accuracy is obtained for reliable marking of deformation areas in a fully automated inspection station, which is able to sustain standard production rates in the automotive industry.

REFERENCES

[1] Y. Lee, S. Park, Y. Jun and W.C. Choi, "A robust approach to edge detection of scanned point data", *International Journal of Advanced Manufacturing Technology*, vol. 23, 2004, pp. 263-271.

[2] M. Pauly, R. Keiser and M. Gross, "Multi-scale feature extraction on point-sampled surfaces", *Computer Graphics Forum*, vol. 22(3), 2003, pp. 281-289.

[3] A. Hubeli and M. Gross, "Multiresolution feature extraction from unstructured meshes", in *Proc. of IEEE Visualization Conf.*, 2001, pp. 287-294.

[4] Y. Yoon, G. DeSouza, and A. Kak, "Real-time tracking and pose estimation for industrial objects using geometric features", in *Proc. of the IEEE Intl. Conf. on Robotics & Automation*, Taiwan, 2003, pp. 3473-3478.

[5] T. Chang, T. Hong, G. Holguinm J. Park, and R. Eastman, "Dynamic 6DOF metrology for evaluating a visual servoing system", in *Proc. of the 2008 Performance Metrics for Intelligent Systems (PerMIS) Workshop*, USA , 2008, pp. 173-180.

[6] C. Harris and M. Stephens, "A combined corner and edge detector", in *Proc. of the 4th Alvey Vision Conference*, UK, 1988, pp. 147–151.

[7] J. Shi and C. Tomasi, "Good features to track", in *Proc. of 9th IEEE Conf. on Computer Vision and Pattern Recognition*, USA, 1994, pp. 593-600.

[8] D. Lowe, "Distinctive image features from scale-invariant keypoints", *Intl. Journal of Computer Vision*, vol. 60, no. 2, 2004, pp. 91-110.

[9] H. Bay, T. Tuytelaars, and L. Van Gool, "SURF: Speeded Up Robust Features", in *Proc. of the ninth European Conference on Computer Vision*, Graz, Austria, May 2006, pp. 404-471.

[10] V. Borsu and P. Payeur, "Pose and motion estimation of a moving rigid body with few features", in *Proc. of the IEEE Intl. Workshop on Robotic and Sensor Environments*, Lecco, Italy, Nov. 2009, pp.116-121.

[11] J.–Y. Bouguet, "Pyramidal implementation of the Lucas Kanade feature tracker – description of the algorithm," [Online], http://robots.stanford. edu/cs223b04/algo_tracking.pdf.

[12] B. D. Lucas and T. Kanade, "An iterative image registration technique with an application to stereo vision", in *Proc. of the 1981 DARPA Imaging Understanding Workshop*, 1981, pp. 121-130.

[13] R. Holt and A. Netravali, "Number of solutions for motion and structure from multiple frame correspondence", *Intl. Journal of Computer Vision*, vol. 23(1), 1997, Kluwer, pp. 5-15.

[14] J. Weng, T. Huang, and N. Ahuja, "Motion and structure from two perspective views:Algorithms, error analysis and error estimation", *IEEE Trans. on Pattern Analysis and Machine Intelligence*, vol. II(5), 1989, pp. 451-476.

[15] A. Yogeswaran and P. Payeur, "Features extraction from point clouds for automated detection of deformations on automotive body parts", in *Proc. of the IEEE Intl. Workshop on Robotic and Sensor Environments*, Lecco, Italy, Nov. 2009, pp.122-127.

[16] A. Boyer, P. Curtis and P. Payeur, "3D Modeling from multiple views with integrated registration and data fusion", in *Proc. of the 6th Canadian Conference on Computer and Robot Vision*, Kelowna, BC, May 2009, pp. 252-259.

[17] R. Hartley and A. Zisserman, *Multiple View Geometry in Computer Vision*, Cambridge University Press, Cambridge, UK, 2000.

[18] K.S. Arun, T.S. Huang, and S.D. Blostein, "Least-squares fitting of two 3-D point set", *IEEE Transactions on Pattern Analysis and Machine Intelligence*, vol.9, no.5, 1987, pp. 698-700.